Delgado-Muñoz, D.; Sanchís, R.; Cecilia, JA.; Rodríguez-Castellón, E.; Caballero, A.; Solsona, B.; López Nieto, JM. (2019). Support effects on NiO-based catalysts for the oxidative dehydrogenation
(ODH) of ethane. Catalysis Today. 333:10-16. https://doi.org/10.1016/j.cattod.2018.07.010

Support effects on NiO-based catalysts for the oxidative dehydrogenation (ODH) of ethane

D. Delgado[a,*], R. Sanchís[b], J. A. Cecilia[c], E. Rodríguez-Castellón[c], A. Caballero[d], B. Solsona[b,*], J.M. López Nieto[a,*]

[a] Instituto de Tecnología Química, Universitat Politècnica de València-Consejo Superior de Investigaciones Científicas, Avenida de los Naranjos s/n, 46022 Valencia, Spain

[b] Department of Chemical Engineering, Universitat de València, Av. Universitat s/n, 46100 Burjassot-Valencia, Spain

[c] Departamento de Química Inorgánica, Facultad de Ciencias, Universidad de Málaga, 29071 Málaga, Spain

[d] Instituto de Ciencia de Materiales de Sevilla (CSIC-University of Seville) and Departamento de Química Inorgánica, University of Seville. Avda. Américo Vespucio, 49. 41092. Seville, Spain

* Corresponding authors, E-mail(s):

dadelmuo@itq.upv.es

Benjamin.Solsona@uv.es

jmlopez@itq.upv.es

Abstract

We report on the effect of NiO-support interactions in the chemical nature of Ni species on a series of supported NiO catalysts for the ODH of ethane. SiO_2, TiO_2-anatase, a high surface area TiO_2 and a porous clay heterostructure (PCH) with TiO_2 and SiO_2 pillars were used as supports, which led to a selectivity to ethylene in the range 30-90 % over supported NiO catalysts. The catalysts were characterized by means of XRD, N_2-Adsorption, H_2-TPR, XPS and in-situ (under H_2 reductive atmosphere) and ex-situ XAS spectroscopy. The catalytic performance of supported materials is discussed in terms of their reducibility and specific reduction kinetics, but also taking into account the specific chemical nature of Ni species on each catalyst. The influence of the particle size and the presence of Ni and O vacancies on the catalytic performance in the ODH of ethane is inferred.

Keywords: Ethylene; Oxidative Dehydrogenation (ODH), Supported NiO, EXAFS

1. Introduction

Ethylene is nowadays a key feedstock for the chemical industry [1]. With a worldwide production of approximately 150 million tons in 2015, it is the precursor of a large variety of commodity chemicals (ethylene oxide, 1,2-dichloroethane, ethylbenzene, etc.), which are the pivotal building blocks for the petrochemical industry [2, 3]. In addition, it is also directly used as building block in the production of polyethylene resins, whose annual production exceeds the 70 million tons per year [4]. However, ethylene is mainly obtained by steam cracking, which is an extremely high energy-demanding process [5, 6]. Considering that ethylene market is steadily growing each year (hand in hand with population growth), the necessity to cope with this increasing demand arises. In this sense, the development of new alternative processes for its production is a recurring topic in catalysis [7-12]. Among all the processes proposed in the last decades, the oxidative dehydrogenation (ODH) of ethane can be considered the most promising one, in view to an industrial implementation [9]. Despite the great efforts devoted to the synthesis of active and selective materials for the ODH of ethane, the catalytic systems that show high activity and selectivity to ethylene are scarce: i) systems based-on MoV mixed oxides (with ethylene yields up to 75 %; and operating at ethane conversions up to 90%) [13-15] or ii) systems based-on NiO (reaching yields to ethylene of ca. 40 %; and operating at ethane conversions lower than 50%) [16-27].

In the case of NiO-based catalysts, several approaches have been proposed to improve the catalytic performance of bulk NiO, which presents a very low selectivity to ethylene (maximum selectivity to ethylene of ca. 30 %) [16]. On the one hand, the use of promoters [16-19], mainly Nb- [16, 17, 20] and Sn- [21-23] (with NiO contents higher than 80 wt. %), can increase the selectivity to ethylene up to 80-90 % at low-medium ethane conversion. On the other hand, supported NiO (using TiO_2 [24], porous clay

heterostructures [25] or Al_2O_3 [26] as supports) can also lead to similar catalytic performance in the ODH of ethane (selectivity to ethylene of ca. 80-90 %).

Despite this, there exists still some controversy about aspects concerning the nature of active and selective sites. For promoted NiO catalysts, it has been reported that the valence of the metal promoter and its acidity can modify NiO surface sites [18]. Also the specific morphology and phase distribution can influence the catalytic performance of these materials [22, 23]. Regarding supported NiO-based catalysts, a key point to take into account is to select the optimum NiO loading to achieve the proper distribution of the active phase [24]. This will lead to the optimum NiO-support interaction to maximize the selectivity to ethylene in the ODH of ethane. Recently Lemonidou et al. reported that the nature of the support could also influence the redox kinetics of NiO-based oxygen transfer materials (OTM´s), which is related to the metal-support interaction strength [27].

The aim of this work is to shed some light on such NiO-support interactions and point out the effects on the reducibility, the reduction kinetics and the nature of Ni species, in order to finally link them with the catalytic performance in the ODH of ethane. We have studied a series of selective supported NiO catalysts: i) NiO supported on anatase TiO_2 ($S_{ethylene}$ = 64 %); ii) NiO supported on a Porous Clay Heterostructure with TiO_2 and SiO_2 pillars ($S_{ethylene}$ = 78 %); iii) on P25 TiO_2 ($S_{ethylene}$ = 89 %)). For comparison, unselective NiO catalysts, (i.e. unsupported and SiO_2-supported NiO, with ca. 30 % selectivity to ethylene) have been also studied. Reducibility and kinetic studies have been carried out by H_2-TPR and time-resolved in-situ XAS spectroscopy, respectively. On the other hand, the chemical nature and environment of the Ni species have been evaluated by means of XPS spectroscopy and EXAFS analysis. The role of particle size and nickel and oxygen vacancies is discussed.

2. Experimental

2.1. Catalysts preparation

Unsupported nickel oxide catalyst (**NiO**) was synthesized by evaporation at 60 ºC of an ethanolic solution of $Ni(NO_3)_2 \cdot 6H_2O$ and oxalic acid (oxalic acid/nitrate molar ratio of 1) to which a solid support was added. Supported NiO catalysts were prepared with different metal oxide supports: a commercial silica (SiO_2), a Porous Clay Heterostructure (PCH) with SiO_2-TiO_2 pillars (PCH-Ti, which its synthesis is reported elsewhere [25]), pure anatase TiO_2 (Sigma-Aldrich) and a high surface area TiO_2 (Degussa P25). All the catalysts were calcined at 500 ºC for 2h. Supported samples were named as **NiO/SiO_2** (10 wt.% NiO), **NiO/PCH-Ti** (17 wt.% NiO), **NiO/Ti-anat** (20 wt.% NiO), and **NiO/Ti-P25** (20 wt.% NiO).

2.2 Catalytic tests

The ethane oxidation catalytic tests were carried out in a tubular isothermal flow reactor at 450 °C. The feed consisted of C_2/O_2/He with a molar ratio of 3/1/26. The usual reaction conditions employed were 100 mg of sample and a total flow rate of 50 ml min^{-1}. Both the amount of catalyst and the total flows were largely varied to get different C_2H_6 conversions at a fixed reaction temperature. The catalysts were introduced in the reactor diluted with silicon carbide in order to keep a constant volume in the catalytic bed. The reactants and reaction products were analyzed by gas chromatography using two packed columns: (i) molecular sieve 5A (2.5 m); and (ii) Porapak Q (3 m). Ethylene and carbon dioxide were the main reaction products detected regardless of the catalyst tested. CO was also identified but with extremely low selectivity (<1%). Blank runs without catalyst (also without CSi) showed no conversion

in the range of reaction temperatures employed. Besides, the carbon balance showed excellent values (±4%) in all the experiments conducted.

2.3. Characterization of the catalysts

Powder X-Ray diffraction (XRD) patterns were collected in an Enraf Nonius FR590 sealed tube diffractometer, equipped with a monochromatic Cu Kα1 radiation source.

XAS experiments in the Ni K-edge were recorded at CLAESS line at ALBA synchrotron light source located in Barcelona (Spain), using an in-house cell developed by ALBA and Instituto de Tecnología Química, which can work under selected atmosphere until 700 ºC. Gases were introduced into the cell using mass flow controllers. The samples were prepared using the optimum mass amount to maximize the signal-to-noise ratio ($Ln(I_0/I_1)\approx1$), which was diluted in boron nitride and pressed into pellets. In-situ time-resolved Ni K-edge XANES spectra were recorded from 8200 to 8490 eV, at a time resolution of c.a. 3 min/spectrum, while spectra for EXAFS analysis were recorded in the range 8200-9175 eV. The software Athena was used for the normalization and the linear combination fitting (LCF) of the spectra, while Artemis was used for EXAFS fitting. The LCF was performed using the calcined samples and metallic Ni as references.

Temperature-programmed reduction experiments (H_2-TPR) were performed in an Autochem 2910 (Micromeritics) equipped with a TCD detector. The reducing gas composition was 10 % H_2 in Ar, with a total flow rate of 50 mL min^{-1}. The materials were heated until 800 ºC at a heating rate of 10 ºC min^{-1}.

X-ray photoelectron spectroscopy was carried out with a non-monochromatic Al Kα (1486.6 eV) X-ray radiation source, in a SPECS spectrometer equipped with a MCD-9 detector. The spectra were acquired using an analyzer pass energy of 50 eV, an X-ray

power of 200 W at a pressure of 10^{-9} mbar. Data processing was carried out with CasaXPS software.

3. Results and discussion

Figure 1 shows the variation of the selectivity to ethylene with ethane conversion in the ODH of ethane at 450 ºC over NiO-based catalysts, whereas Table 1 summarizes the catalytic performance. Unsupported **NiO** and **NiO/SiO$_2$** displayed the lowest selectivity to ethylene (ca. 30 %). When NiO is supported on Ti-containing materials, a drastic increase in the selectivity to ethylene is observed, reaching values of approximately 89 % for **NiO/Ti-P25** catalyst (Fig.1) (Table 1). Besides this increment in selectivity to ethylene, it is worth mentioning that the ethylene formed displayed a very low reactivity in the studied conversion range, even for the less selective catalysts **NiO** and **NiO/SiO$_2$**. CO_2 was the only by-product found during the reaction in all the catalysts tested, which seems to be formed directly from ethane, since no changes in the selectivity to ethylene with ethane conversion have been observed. Interestingly, CO, which is usually formed by overoxidation of ethylene [7], has not been detected. It is possible that the no observation of CO could be due to the high reactivity towards CO oxidation to CO_2, which can take place at temperatures remarkably lower than those used in our experiments. In fact, NiO particles are capable of oxidizing CO even at room temperature [28, 29]. We must point out the high ethylene stability observed on nickel-based catalysts at moderate ethane conversions, which is in agreement with previous results over NiO systems [15-27]. This has also been reported for catalysts based on MoV mixed oxides with the M1-phase structure [13-15].

In addition, supported materials presented much higher catalytic activity than unsupported **NiO**, despite their lower NiO loading (Table 1).

Figure 2A displays powder XRD profiles of NiO-based catalysts. All the patterns show the characteristic diffraction lines corresponding to Fm3m NiO cubic phase (ICSD: 184626), which is present as the only crystalline nickel-containing phase in the materials (Fig. 2A). Supported catalysts show additional Bragg signals corresponding to the specific supports, except for amorphous SiO_2-supported sample **NiO/SiO$_2$**, which just shows nickel oxide diffraction peaks (Fig. 2A, pattern c). In the case of TiO_2-supported catalysts, the main crystalline phase observed was anatase-type TiO_2 (JCPDS: 84-1286) (Fig.2A, patterns d and e), although small amounts of rutile-type phase (JCPDS: 82-0514) are also present in **NiO/Ti-P25** catalyst (Fig. 2A, pattern e). Additionally, no appreciable shifts in NiO diffraction lines have been observed, which indicates that the cubic cell parameter must remain constant in all the series of catalysts (Fig. 2A). Unsupported **NiO** displays narrower diffraction lines with respect to supported catalysts, which indicates a higher crystallinity and a bigger particle size (Fig. 2A, pattern a). In fact, average particle size was estimated from FWMH values using Scherrer's equation, which shows a smaller particle size in the case of supported materials (Table 1). According to this, high surface area supports seem to favor the formation of small crystallite size NiO particles (Table 1). Moreover, the catalytic activity of the studied catalysts is directly related to NiO crystallite size, being higher as the NiO particle size decreases (Fig. 2B).

Temperature-programmed reduction experiments under H_2 atmosphere (H_2-TPR) were conducted in order to study the reducibility of the titled materials (Fig. 3). Attending to the temperature for the maximum consumption of H_2 observed for each catalyst (TMC), the reducibility decreases in the following trend: **NiO/SiO$_2$** > **NiO** ≈ **NiO/Ti-P25** > **NiO/Ti-anat** > **NiO/PCH-Ti**. Nevertheless, H_2-TPR profiles show several H_2 uptake signals for all the catalysts studied, which can be assigned to the presence of Ni species

with different reducibility (Fig. 3). Unsupported **NiO** shows two main H_2 consumption peaks, which can be ascribed to a two-step reduction mechanism: $Ni^{2+} \rightarrow Ni^{\delta+} \rightarrow Ni^0$ (Fig. 3, pattern a) [30]. This mechanism can be explained in terms of NiO particle size and diffusion of the reductant into the nickel oxide matrix. In this sense, bigger crystallite size would increase the relative intensity of the signal appearing at higher temperatures, mainly due to problems of H_2 diffusion. This observation points out the importance of the morphology and microstructure of the materials in the reducibility. In fact, the particular phase distribution in each catalyst (i.e. the distribution of the active phase and the support) can also impede the reduction of NiO, as it has been observed in Sn-promoted NiO [23]. This could be the case of **NiO/PCH-Ti,** in which the reduction of NiO located within interlayer pores must be hindered with respect to well accessible NiO particles (Fig. 3, pattern c). Additionally, signals at ca. 400 ºC have been reported to be due to the presence of surface Ni-support mixed phases (i.e. Ni(II) titanates or silicates), which would show much lower reducibility than NiO [31]. These signals are mainly observed in **NiO/SiO_2** and **NiO/Ti-P25** (Fig. 3, patterns b and e). Also signals at lower temperatures (200-250 ºC) are found, which could be ascribed to the presence of non-stoichiometric NiO, since it shows a lower activation energy for starting the catalytic nucleation (Fig. 3, patterns b and c) [32]. This heterogeneity in terms of reducibility of Ni species observed along the entire series makes it a little adventurous to ascribe the catalytic performance of the materials only to their reducibility under H_2 atmosphere. Despite this, a low reducibility seems to favor a higher selectivity to ethylene.

In addition, it is possible to evaluate the reaction kinetics during the reduction under H_2 at a fixed temperature (450 ºC) by the in-situ analysis of the changes in the characteristic features of the XANES Ni K-edge spectra of the materials (Fig. 4). These

features consist of a high intensity signal at 8349 eV (known as white line) and a low intensity shoulder at 8334 eV in the case of NiO; and a very low intensity white line at 8349 eV and a high intensity peak at 8334 eV, in the case of metallic Ni (Fig. 4A and Fig. 4B) [33]. The analysis by linear combination fitting (LCF) of each recorded spectrum (Fig. 4B) using metallic Ni and the fresh catalysts as references, gives rise to the kinetic curves displayed in Figure 5. It can be observed that unsupported **NiO** and **NiO/SiO$_2$** display the fastest reduction kinetics among the catalysts studied (Fig. 5), which resulted to be the less selective catalysts for the ethane ODH (Table 1). On the other hand, **NiO/PCH-Ti** shows the slowest rate for the reduction by H_2, which is in line with the results obtained by H_2-TPR. **NiO/Ti-P25** also displays a slower reduction rate than that of unsupported **NiO** and **NiO/SiO$_2$**. In this way, slower reduction kinetics seem to favor a higher selectivity to ethylene. This would ensure a more controlled oxygen supply, avoiding deep oxidation to CO_2.

Figure 6A shows Ni $2p_{3/2}$ core level XPS spectra of NiO-based catalysts. All the spectra present a main peak at ca. 853-854 eV which present a line-broadening, which can be considered as an additional contribution (at approximately 1.5 eV over the main line). This additional contribution, known as satellite peak I (Sat-I) has been ascribed to non-local screening effects [34], but also to the presence of several structural defects like Ni^{2+} vacancies [35], Ni^{3+} cations [36, 37] or Ni^{2+}-OH species [38]. Also another broad contribution is present at approximately 7 eV over the main peak, which is usually attributed to ligand-metal charge transfer, and known as shake-up satellite or satellite peak II (Sat-II) [34, 35, 38]. All the supported samples present an extra low intensity band below the main peak (marked with an asterisk in Fig. 6A), which can be assigned to differential charging on the samples provoked by heterogeneities in the electrical conductivity, likely due to active phase-support interactions [39, 40]. The intensity ratio

between satellite peaks and the main peak can be used to obtain information about the surface species present in the materials [41, 42]. In fact, Sat-I/main peak ratio is very dependent on the number of defects and NiO particle size [34-38]. In this sense, supported catalysts present much lower Sat I/ Main peak ratio than unsupported **NiO** (Table 2). This fact has also been observed in other NiO-based catalytic systems, either in supported or promoted catalysts, which can be attributed to changes in the surface Ni environment, mainly due to the generation of defects or changes in the particle size due to the interaction with the promoter or the support [21, 24, 25]. It appears difficult to separate the contribution of both parameters (defects and particle size) to satellite peaks. Accordingly, the selectivity to ethylene increases proportionally with Sat-I/main peak ratio just for Ti-containing catalysts, suggesting that the presence of defects could play a significant role in the catalytic performance of this type of materials (Fig. 6B).

Figure 7A shows the Fourier Transform (F.T.) of the EXAFS Ni K-edge region of NiO catalysts, which can be used to study the short-range environment of Ni-species in the materials. No appreciable differences in the Ni-O and Ni-Ni distances are observed (1^{st} and 2^{nd} Coordination Shells respectively), being similar along all the series (Fig. 7A) (Table 2). However, slight changes in the relative intensities in the F.T. of the EXAFS region of Ni-O and Ni-Ni shells can be noted depending on the catalyst (Fig. 7A). This suggests changes in the coordination environment of Ni, i.e. coordination number in both analyzed shells. The specific coordination numbers of Ni on each catalyst were calculated from the amplitude reduction factors (S_0^2) extracted from EXAFS fittings, using unsupported **NiO** catalyst as a reference. Thus, when NiO is supported, both Ni-O and Ni-Ni coordination numbers decrease with respect to unsupported **NiO** (Table 2). This fact is more significant when Ti-containing supports are used, suggesting either a higher interaction between NiO and TiO_2, which could generate a higher number of Ni

and O vacancies. However, the differences observed in the first coordination shell (Ni-O) could be also due to a disordered octahedral environment caused by a smaller particle size, rather than to a real decrease in the number of oxygen neighbors (Table 2) [43]. Figure 7B and Figure 7C show the variation of the selectivity to ethylene with coordination number of Ni for the 1st and 2nd coordination shells (Ni-O and Ni-Ni respectively). A correlation between Ni environments and selectivity to ethylene can be outlined. Thus, the selectivity to ethylene increases as the coordination number for the first and second shells decreases (Fig. 7B and Fig. 7C). Although the correlation with with Ni-O coordination number is not as evident as in the case of Ni-Ni shell, the number of Ni-O and Ni-Ni neighbors in the best catalysts seems to be much lower. Hence, these results suggest that high selectivity to ethylene could be directly related with the elimination of non-selective sites, i.e. with the generation of Ni and O vacancies, likely due to NiO-support interactions.

4. Conclusions

The effect of the support in the catalytic properties of supported NiO catalysts for the ODH of ethane has been studied. Depending on the support, NiO with different physicochemical features have been obtained. Unsupported and SiO_2-supported NiO displayed the lowest selectivity to ethylene (ca. 30 %). However, a substantial increase in the selectivity to ethylene (reaching values in the range 64-85%) is observed when NiO is supported on Ti-containing materials, i.e. on TiO_2 or on porous clay heterostructure with SiO_2-TiO_2 pillars (PCH-Ti). In addition, carbon dioxide is the only deep oxidation product, indicating the relatively low reactivity of ethylene over our catalysts. The nature of the support in NiO-supported catalysts leads to the modification of the chemical nature of NiO and this strongly affects the catalytic performance. In

fact, it has been found that the catalytic activity of the catalysts increases as the NiO crystallite size decreases, being directly related to the number of active sites exposed on the surface. But, in addition, the support can also modify the chemical nature of NiO, what plays a key role in the catalytic performance. Studies on the reducibility of the materials (carried out by H_2-TPR and time-resolved in-situ XAS experiments under H_2 atmosphere) show that Ti-containing catalysts present lower reducibility and slower reduction kinetics than unsupported and SiO_2-supported NiO. This can have an influence on the increment of selectivity to ethylene, since low reducibility and slow reduction kinetic can ensure a more controlled oxygen supply during the ODH of ethane, favoring ethylene formation. However, the samples present certain heterogeneity in the type of Ni species, showing sites with low, medium and high reducibility (deduced from H_2-TPR analyses). Additionally, we have studied the nature of surface Ni species and Ni environment in the materials by XPS and EXAFS analysis. Both techniques suggest an important role of defects, mainly Ni and O vacancies, on the catalytic behavior of catalysts. Particularly, the increase in the selectivity to ethylene in Ti-containing catalysts can be directly related with the increment of the number of Ni and O vacancies in the catalysts.

Acknowledgements

Authors would like to thank the DGICYT in Spain CTQ2015-68951-C3-1-R, CTQ2015-68951-C3-3-R, CTQ2012-37925-C03-2 and ENE2017-88818-C2-1-R. Also authors want to acknowledge the ALBA Synchrotron Light Source (Project ID: 2015021258 at CLAESS beamline). Authors from ITQ thank Project SEV-2016-0683 for financial support. D.D. also thanks MINECO and Severo Ochoa Excellence Program for his fellowship (SVP-2014-068669). Authors from UV thank the University

of Valencia (UV-INV-AE16-484416 project) and MINECO (MAT2017-84118-C2-1-R project) for funding.

References

[1] M. Ghanta, D. Fahey, B. Subramaniam, App. Pet. Res. 4 (2014) 167-179.

[2] D. Lippe, Oil Gas J. 114 (2016) 62-70.

[3] T.J. Farmer, M. Mascal, Platform Molecules, Introduction to Chemicals from Biomass, John Wiley & Sons, Ltd., 2015, pp. 89-155.

[4] R.A. Collins, A.F. Russell, P. Mountford, App. Pet. Res. 5 (2015) 153-171.

[5] J.J.H.B. Sattler, J. Ruiz-Martinez, E. Santillan-Jimenez, B.M. Weckhuysen, Chem. Rev. 114 (2014) 10613-10653.

[6] H. Arakawa, M. Aresta, J.N. Armor, M.A. Barteau, E.J. Beckman, A.T. Bell, J.E. Bercaw, C. Creutz, E. Dinjus, D.A. Dixon, K. Domen, D.L. DuBois, J. Eckert, E. Fujita, D.H. Gibson, W.A. Goddard, D.W. Goodman, J. Keller, G.J. Kubas, H.H. Kung, J.E. Lyons, L.E. Manzer, T.J. Marks, K. Morokuma, K.M. Nicholas, R. Periana, L. Que, J. Rostrup-Nielson, W.M.H. Sachtler, L.D. Schmidt, A. Sen, G.A. Somorjai, P.C. Stair, B.R. Stults, W. Tumas, Chem. Rev. 101 (2001) 953-996.

[7] C.A. Gärtner, A.C. van Veen, J.A. Lercher, ChemCatChem, 5 (2013) 3196-3217.

[8] M.M. Bhasin, J.H. McCain, B.V. Vora, T. Imai, P.R. Pujadó, Appl. Catal. A: Gen 221 (2001) 397-419.

[9] F. Cavani, N. Ballarini, A. Cericola, Cat. Today 127 (2007) 113-131.

[10] M. Zhang, Y. Yu, Dehydration of Ethanol to Ethylene, Ind. Eng. Chem. Res. 52 (2013) 9505-9514.

[11] S.P. Pyl, C.M. Schietekat, M.-F. Reyniers, R. Abhari, G.B. Marin, K.M. Van Geem, Chem. Eng. J. 176-177 (2011) 178-187.

[12] T. Dijkmans, S.P. Pyl, M.-F. Reyniers, R. Abhari, K.M. Van Geem, G.B. Marin, Green Chem. 15 (2013) 3064-3076.

[13] J.M. Lopez Nieto, P. Botella, M.I. Vazquez, A. Dejoz, Chem. Commun. (2002) 1906-1907.

[14] P. Botella, A. Dejoz, M.C. Abello, M.I. Vázquez, L. Arrúa, J.M. López Nieto, Cat. Today 142 (2009) 272-277.

[15] P. Botella, E. García-González, A. Dejoz, J.M. López Nieto, M.I. Vázquez, J. González-Calbet, J. Catal. 225 (2004) 428-438.

[16] E. Heracleous, A.A. Lemonidou, J. Catal. 237 (2006) 162-174.

[17] E. Heracleous, A.A. Lemonidou, J. Catal. 237 (2006) 175-189.

[18] J.M. López Nieto, B. Solsona, R.K. Grasselli, P. Concepción, Top. Catal. 57 (2014) 1248-1255.

[19] H. Zhu, D.C. Rosenfeld, M. Harb, D.H. Anjum, M.N. Hedhili, S. Ould-Chikh, J.-M. Basset, ACS Catal. 6 (2016) 2852-2866.

[20] B. Savova, S. Loridant, D. Filkova, J.M.M. Millet, Appl. Catal. A: Gen 390 (2010) 148-157.

[21] B. Solsona, P. Concepción, B. Demicol, S. Hernández, J.J. Delgado, J.J. Calvino, J.M. López Nieto, J. Catal. 295 (2012) 104-114.

[22] B. Solsona, J.M. López Nieto, S. Agouram, M.D. Soriano, A. Dejoz, M.I. Vázquez, P. Concepción, Top. Catal. 59 (2016) 1564-1572.

[23] D. Delgado, B. Solsona, A. Ykrelef, A. Rodríguez-Gómez, A. Caballero, E. Rodríguez-Aguado, E. Rodríguez-Castellón, J. Phys. Chem. C 121 (2017) 25132-25142.

[24] R. Sanchis, D. Delgado, S. Agouram, M.D. Soriano, M.I. Vázquez, E. Rodríguez-Castellón, B. Solsona, J.M.L. Nieto, Appl. Catal. A: Gen 536 (2017) 18-26.

[25] B. Solsona, P. Concepcion, J.M. Lopez Nieto, A. Dejoz, J.A. Cecilia, S. Agouram, M.D. Soriano, V. Torres, J. Jimenez-Jimenez, E. Rodriguez-Castellon, Catal. Sci. Technol. 6 (2016) 3419-3429.

[26] E. Heracleous, A.F. Lee, K. Wilson, A.A. Lemonidou, J. Catal. 231 (2005) 159-171.

[27] D. Ipsakis, E. Heracleous, L. Silvester, D.B. Bukur, A.A. Lemonidou, Chem. Eng. J. 308 (2017) 840-852.

[28] S.W. Han, D.H. Kim, M.G. Jeong, K.J. Park, Y.D. Kim, Chem. Eng. J. 283 (2016) 992–998.

[29] M.G. Jeong, I.H. Kim, S.W. Han, D.H. Kim, Y.D. Kim, J. Mol. Catal. A 414 (2016) 87–93.

[30] W. Shan, M. Luo, P. Ying, W. Shen, C. Li, Appl. Catal. A: Gen 246 (2003) 1-9.

[31] L. Zhang, J. Lin, Y. Chen, J. Chem. Soc. Faraday Trans. 88 (1992) 2075-2078.

[32] F. Medina, P. Salagre, J.L.G. Fierro, J.E. Sueiras, J. Catal. 142 (1993) 392-405.

[33] J. Sa, Y. Kayser, C.J. Milne, D.L. Abreu Fernandes, J. Szlachetko, Phys. Chem. Chem. Phys. 16 (2014) 7692-7696.

[34] V. Biju, M. Abdul Khadar, J. Nanopart. Res. 4 (2002) 247-253.

[35] V.M.A. van, Sawatzky, Phys Rev. Lett. 70 (1993) 2459-2462.

[36] P. Salagre, J.L.G. Fierro, F. Medina, J.E. Sueiras, J. Mol. Catal. A: Chem. 106 (1996) 125-134.

[37] M. Tomellini, J. Chem. Soc., Faraday Trans. 1, 84 (1988) 3501-3510.

[38] J.C. Vedrine, G. Hollinger, M.D. Tran, J. Phys. Chem. 82 (1978) 1515-1520.

[39] A. Fernandez, J.P. Espinos, D. Leinen, A.R. Gonzalez-Elipe, J.M. Sanz, Surf. Interface Anal. 22 (1994) 111-114.

[40] Y.V. Larichev, B.L. Moroz, V.I. Bukhtiyarov, Appl. Surf. Sci. 258 (2011) 1541-1550.

[41] G.C. Allen, S.J. Harris, J.A. Jutson, J.M. Dyke, Appl. Surf. Sci. 37 (1989) 111-134.

[42] A.R. Gonzalez-Elipe, J.P. Holgado, R. Alvarez, G. Munuera, J. Phys. Chem. 96 (1992) 3080-308.

[43] D.C. Koningsberger, Stereo chemistry and electronic structure XAFS spectroscopy: Data-analysis and applications, Neutron and synchrotron radiation for condensed matter studies, Volume II, Applications to solid state physics and chemistry, Springer-Verlag Berlin Heidelberg, 1994, pp. 213-244.

Table 1: Main Characteristics and Catalytic performance in the ODH of ethane of NiO-based catalysts.

Catalyst	**NiO loading (wt%)** [a]	**Support type**	**Support Phase**	**NiO particle size (nm)**[c]	**BET surface area (m^2 g^{-1})**[d]	**Catalytic Activity** [e]	**Selectivity to ethylene (%)**[f]
NiO	100	n.s.[b]	n.s.	30.0	15	1117	33
NiO/SiO_2	10	SiO_2	Amorphous	12.6	168	5080	30
NiO/PCH-Ti	17	PCH-Ti	PCH-Ti	6.2	360	10941	78
NiO/Ti-anat	20	TiO_2	Anatase	13.1	26	5725	64
NiO/Ti-P25	20	TiO_2	Anatase + Rutile	19.4	50	5400	89

a) Calculated by Energy-Dispersive X-ray spectroscopy; b) not supported; c) Obtained by means of Scherrer equation; d) Calculated by Brauner-Emmet-Teller method from N_2-adsorption isotherms; e) Catalytic activity at 450 ºC and conversions lower than 5% in g_{C2H6} kg_{NiO}^{-1} h^{-1}; f) At a ethane conversion of 10 % and a reaction temperature of 450 ºC

Table 2: EXAFS and XPS results of NiO-based catalysts.

Catalyst	**NiO loading (wt %)**[a]	**EXAFS**[b]				**XPS**[d]		
		1st Shell (Ni-O)		**2nd Shell (Ni-Ni)**		**Surface**	**SI/Main peak**	**SII/Main peak**
		N[c]	**d_{Ni-O} (Å)**	**N**	**d_{Ni-O} (Å)**	**at. Ni/(Ti+Si)**		
NiO	100	6.00	2.08	12.00	2.95	-	4.07	3.90
NiO/SiO_2	10	6.00	2.08	11.60	2.95	0.04	1.36	1.96
NiO/PCH-Ti	17	5.72	2.08	10.68	2.95	0.42	1.46	1.57
NiO/Ti-anat	20	5.29	2.08	10.92	2.95	0.28	1.33	0.84
NiO/Ti-P25	20	5.15	2.08	10.44	2.95	0.46	1.58	1.99

a) Calculated by Energy-Dispersive X-ray spectroscopy; b) Extended X-ray Absorption Fine Structure; c) Coordination number; d) X-ray Photoelectron Spectroscopy.

Caption to Figures

Figure 1. Variation of the selectivity to ethylene with ethane conversion for NiO-based catalysts. Symbols: NiO (▲), NiO/SiO_2 (■), NiO/PCH-Ti (▽), NiO/Ti-anat (●), NiO/Ti-P25 (○).

Figure 2. XRD patterns of NiO-based catalysts (A) and catalytic activity as a function of NiO particle size (B) of the catalysts: a) NiO, b) NiO/SiO_2, c) NiO/PCH-Ti, d) NiO/Ti-anat, and e) NiO/Ti-P25. Symbols: NiO (●), PCH-Ti (▽), TiO_2-anatase (■), TiO_2-rutile (▲).

Figure 3. H_2-TPR profiles of NiO-based catalysts. a) NiO, b) NiO/SiO_2, c) NiO/PCH-Ti, d) NiO/Ti-anat, and e) NiO/Ti-P25.

Figure 4. Ni K-edge XANES spectra of NiO and metallic Ni (A) and Time-resolved XANES spectra in the Ni K-edge region of NiO-based catalysts during the reduction under H_2 atmosphere (B): a) NiO, b) NiO/SiO_2, c) NiO/PCH-Ti, and d) NiO/Ti-P25. Reduction conditions: T=450 ºC; H_2/He, 25/25 (mL min^{-1}).

Figure 5. Kinetic curves of reduction in H_2 calculated by linear combination fitting of the corresponding time-resolved Ni K-edge spectra (Reduction conditions as in Fig. 4). Symbols: NiO (▲), NiO/SiO_2 (■), NiO/PCH-Ti (▽), NiO/Ti-P25 (○)

Figure 6. Ni $2p_{3/2}$ core level XPS spectra of NiO-based catalysts (A) and variation of selectivity to ethylene as a function of Ni $2p_{3/2}$ core level XPS Satellite I/Main peak

ratio: a) NiO, b) NiO/SiO_2, c) NiO/PCH-Ti, d) NiO/Ti-anat, and e) NiO/Ti-P25. Symbols: Ti-containing catalysts (●), Unpromoted NiO (△), NiO/SiO_2 (□).

Figure 7. Fourier Transform of EXAFS Ni K-edge region of NiO-based catalysts (A) and variation of selectivity to ethylene as a function of Ni-O coordination number calculated by EXAFS fitting (B) or as a function of Ni-Ni coordination number calculated by EXAFS fitting (C). Catalysts: a) NiO, b) NiO/SiO_2, c) NiO/PCH-Ti, d) NiO/Ti-anat, and e) NiO/Ti-P25. Symbols: Ti-containing catalysts (●), Unpromoted NiO (△), NiO/SiO_2 (□).

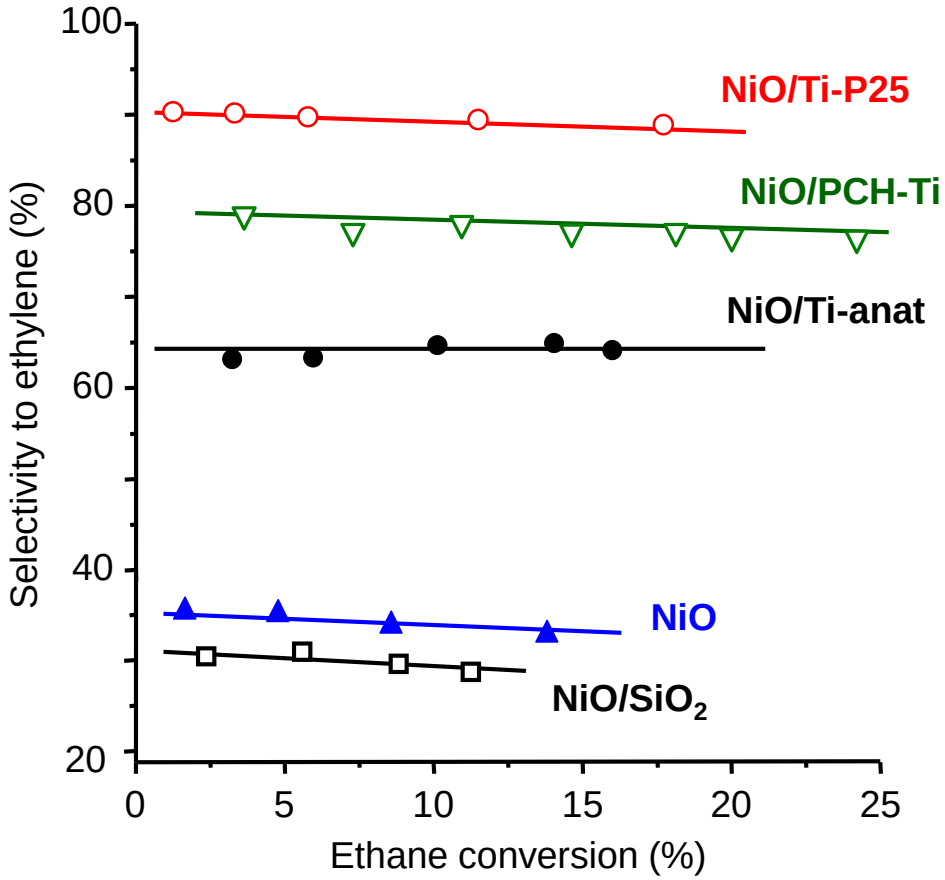
100
80
60
40
20
Selectivity to ethylene (%)
0
5
10
15
20
25
Ethane conversion (%)
NiO/Ti-P25
NiO/PCH-Ti
NiO/Ti-anat
NiO
NiO/SiO2

Figure 1

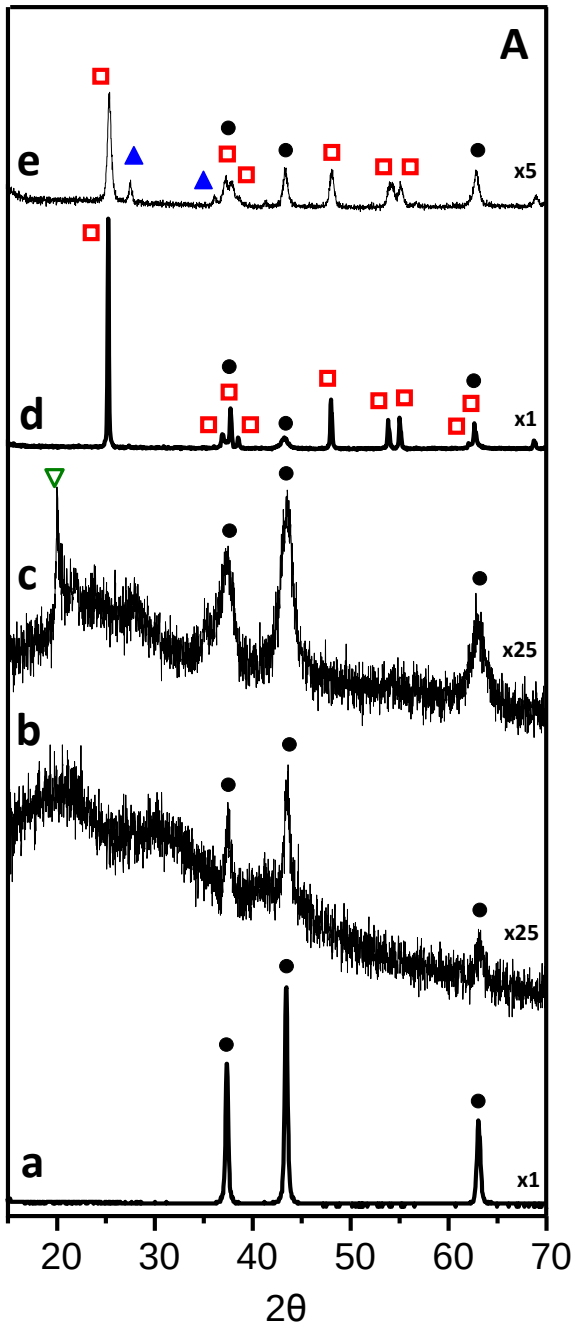
A
e
x5
d
x1
c
x25
b
x25
a
x1
20
30
40
50
60
70
2θ

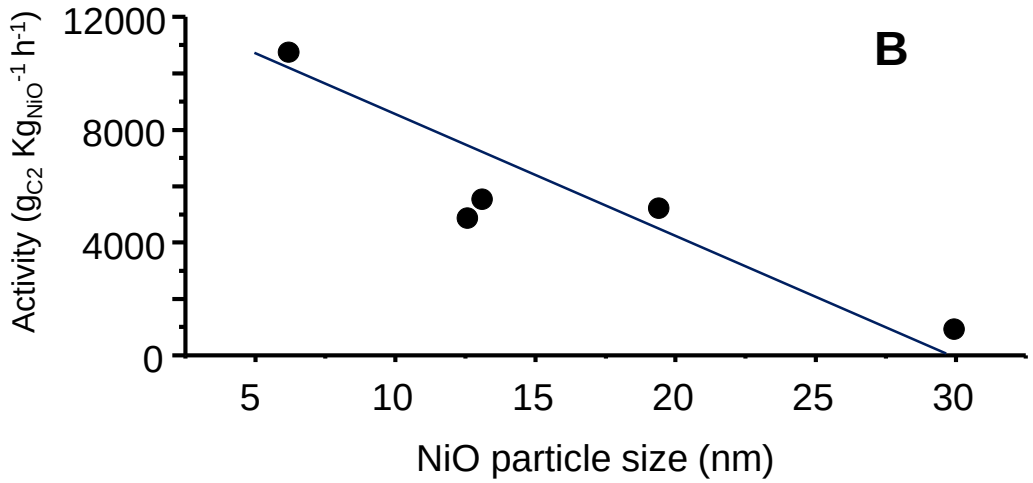
B
Activity (g_{C2} Kg_{NiO}^{-1} h^{-1})
12000
8000
4000
0
5
10
15
20
25
30
NiO particle size (nm)

Figure 2

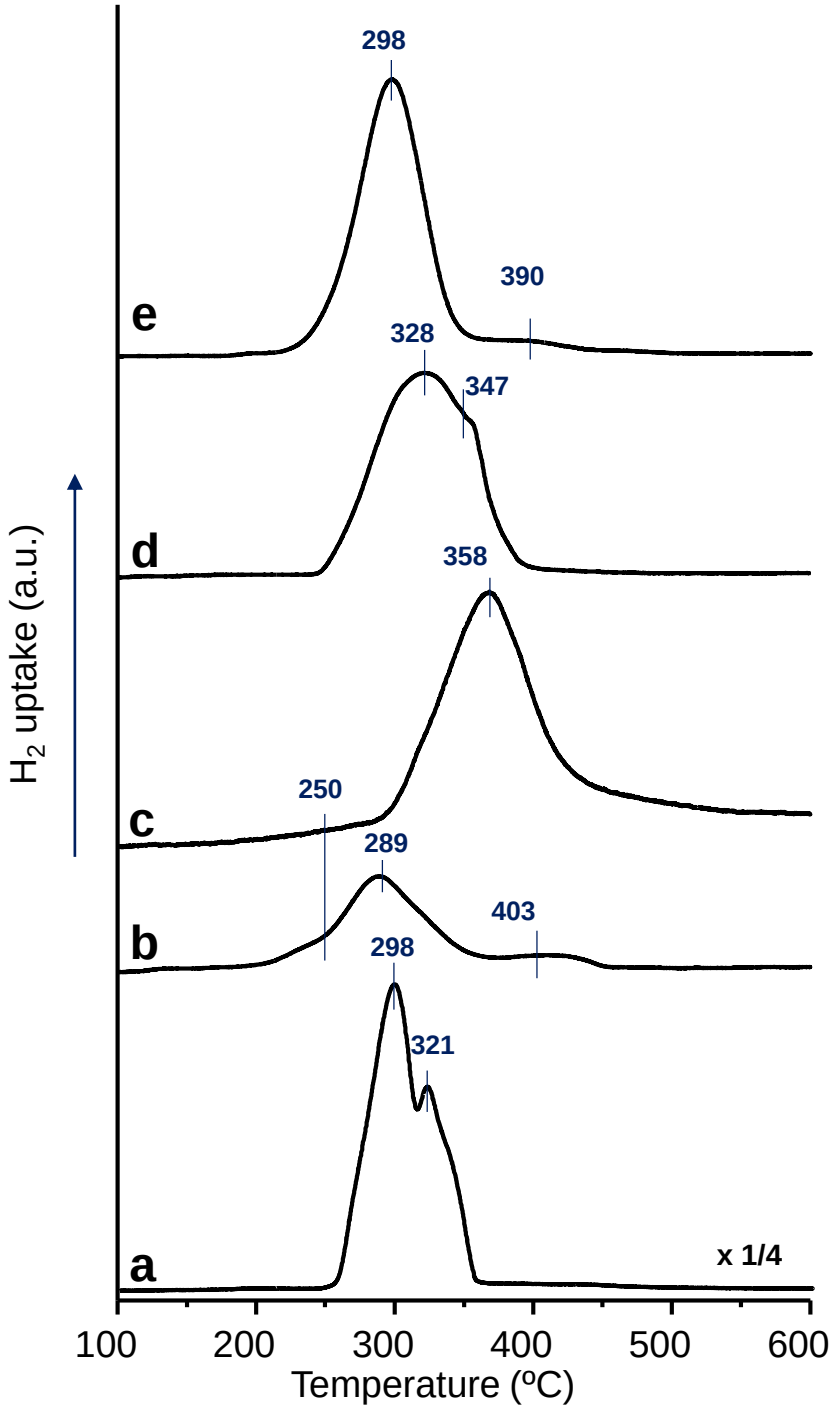
298
390
e
328
347
d
358
250
c
289
403
b
298
321
a
x 1/4
H2 uptake (a.u.)
100
200
300
400
500
600
Temperature (ºC)

Figure 3

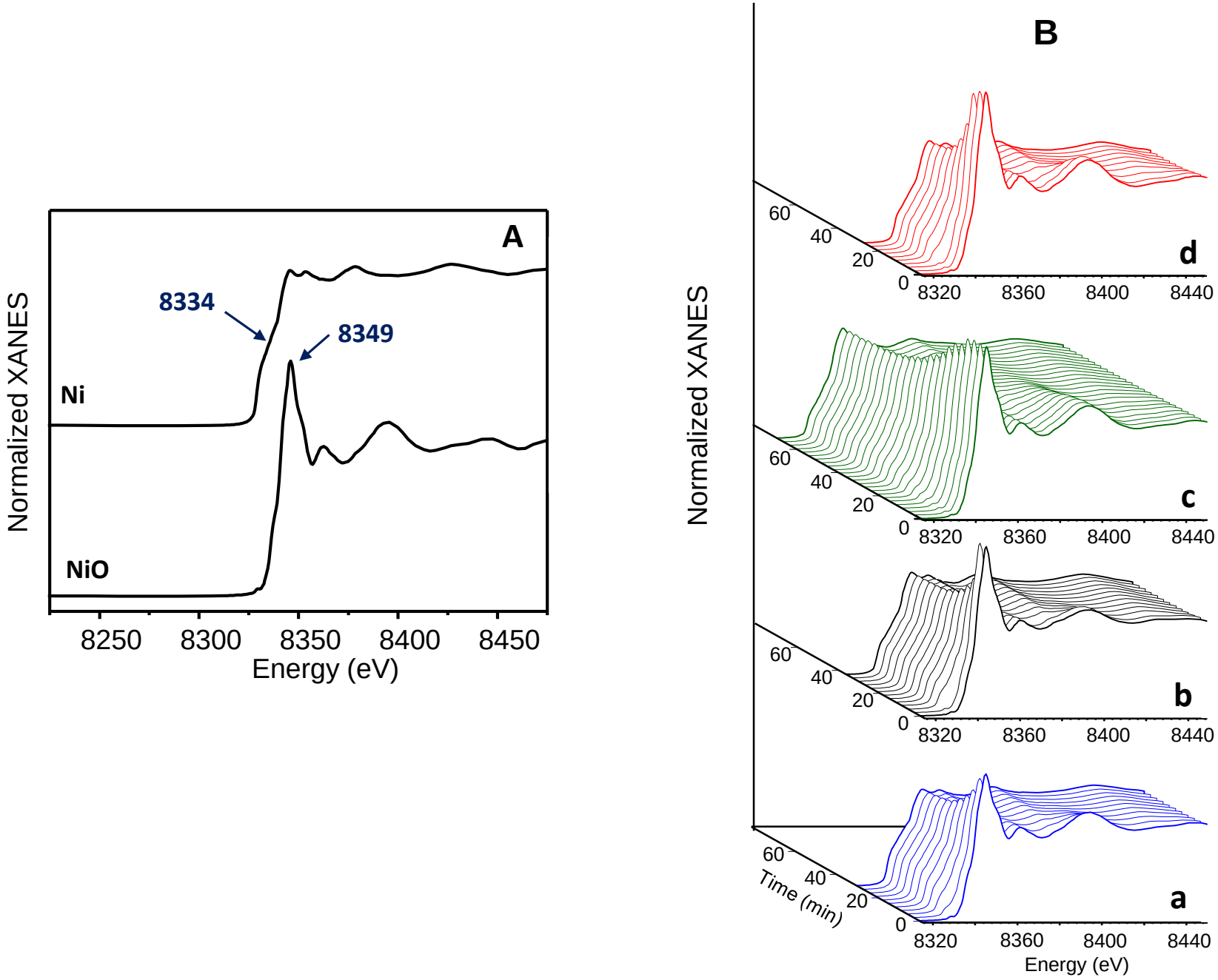
A
8334
8349
Ni
NiO
Normalized XANES
8250
8300
8350
8400
8450
Energy (eV)
B
Normalized XANES
d
c
b
a
60
40
20
0
8320
8360
8400
8440
Time (min)
Energy (eV)

Figure 4

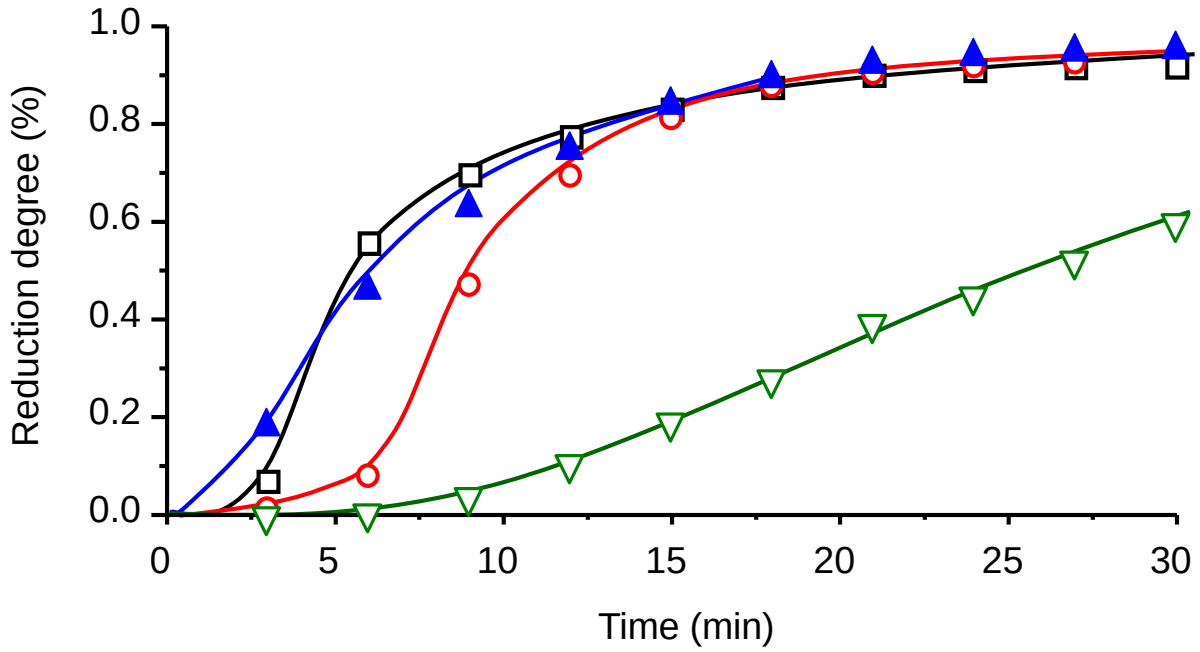

Figure 5

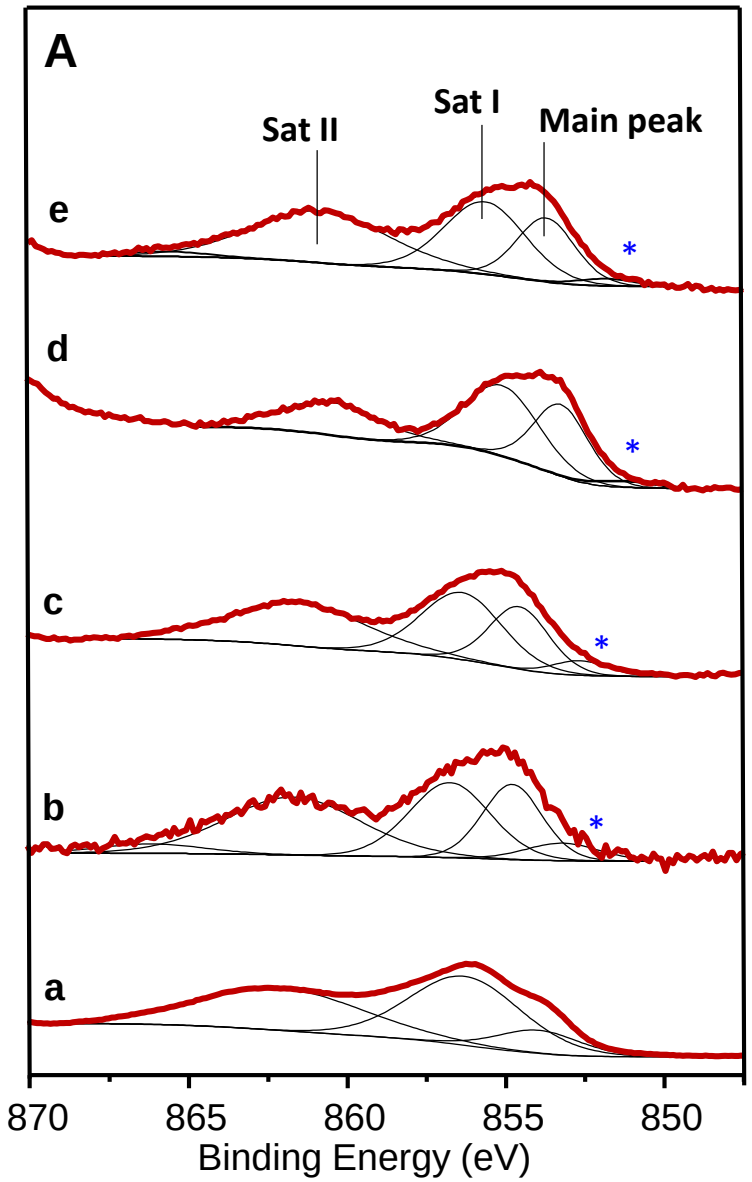
A
Sat II
Sat I
Main peak
e
d
c
b
a
*
870
865
860
855
850
Binding Energy (eV)

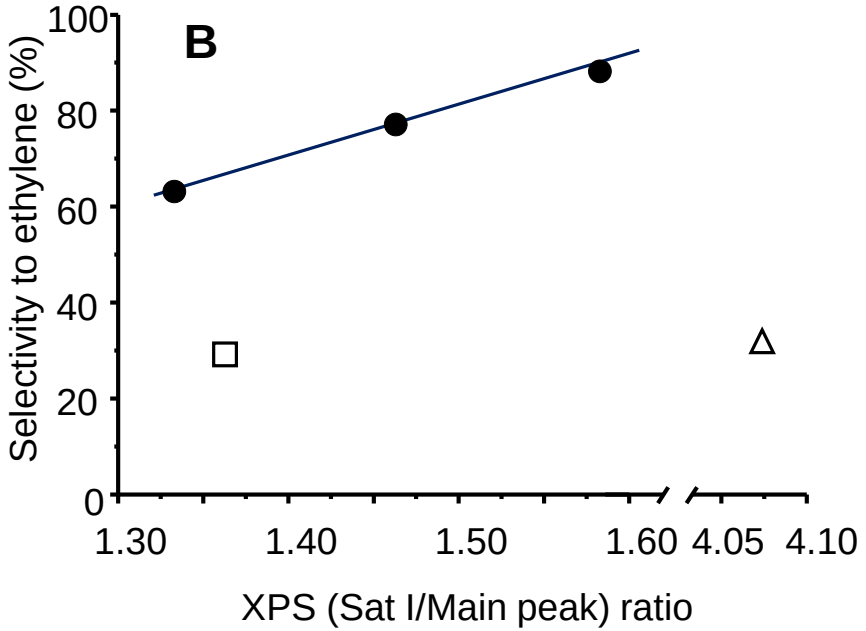
B
Selectivity to ethylene (%)
100
80
60
40
20
0
1.30
1.40
1.50
1.60
4.05
4.10
XPS (Sat I/Main peak) ratio

Figure 6

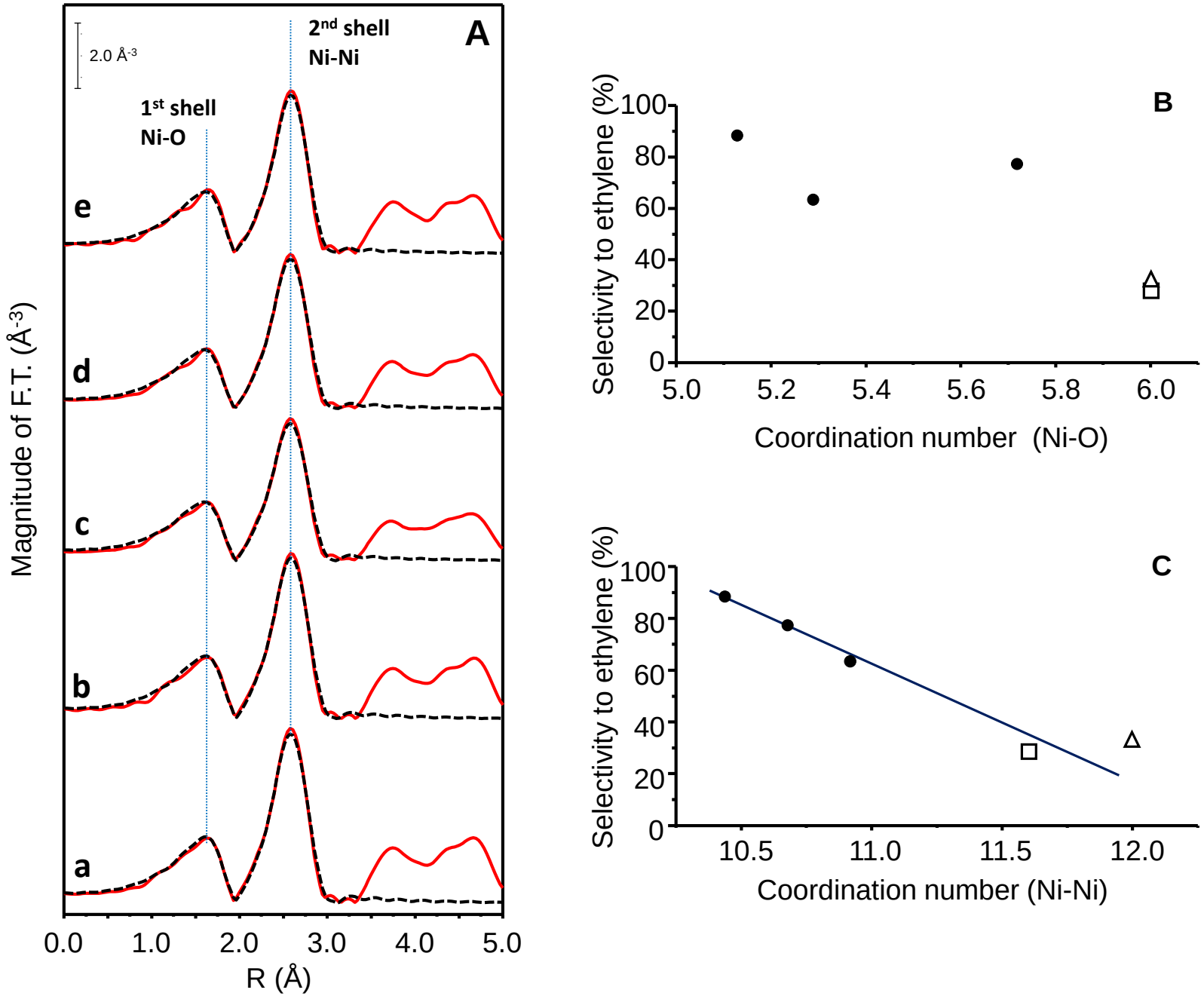
A
2.0 Å-3
2nd shell
Ni-Ni
1st shell
Ni-O
e
d
c
b
a
Magnitude of F.T. (Å-3)
0.0
1.0
2.0
3.0
4.0
5.0
R (Å)
B
Selectivity to ethylene (%)
100
80
60
40
20
0
5.0
5.2
5.4
5.6
5.8
6.0
Coordination number (Ni-O)
C
Selectivity to ethylene (%)
100
80
60
40
20
0
10.5
11.0
11.5
12.0
Coordination number (Ni-Ni)

Figure 7